Electronic Supplementary Information (ESI)

Selective Adsorption and Separation of C_2 Hydrocarbons in a "Flexible-Robust" Metal-Organic Framework on Guest-Dependent Gate-Opening Effect

Peng-Dan Zhang,‡ Xue-Qian Wu,‡ Tao He, Lin-Hua Xie, Qiang Chen, and Jian-Rong Li*

Beijing Key Laboratory for Green Catalysis and Separation and Department of Chemistry and Chemical Engineering, College of Environmental and Energy Engineering, Beijing University of Technology, Beijing 100124, P. R. China.

Table S1. The physical parameters of C_2 hydrocarbon molecules[1-3]

Compounds	Space filling model	Dimensions (Å^3)	Kinetic diameter (Å)	Boiling point (K)
Carbon dioxide (CO_2)	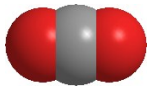	3.19 × 3.34 × 5.36	3.3	194.7
Acetylene (C_2H_2)	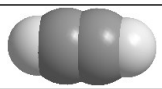	3.32 × 3.34 × 5.70	3.3	189.3
Ethylene (C_2H_4)	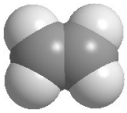	3.28 × 4.18 × 4.84	4.2	169.5
Ethane (C_2H_6)	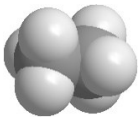	3.81 × 4.08 × 4.82	4.4	184.6

Experimental section

All reagents were purchased directly and used as received.

Synthesis of $Zn_2(Atz)_2Ox$

$Zn_2(Atz)_2Ox$ was synthesized and activated based on the previously reported procedures with minor modification.[4] A mixture of zinc acetate (0.079 g, 0.36 mmol), amino-triazole (0.040 g, 0.44 mmol), oxalic acid (0.16 g, 1.90 mmol), deionized water (20 mL), and butyl alcohol (4 mL) was placed in a Teflonlined stainless steel vessel (70 mL) and stirred for 30 min to get homogeneous substance. The reaction system was then heated at a rate of 5 °C min^{-1} to 180 °C and kept at that temperature for 60 h, and then it was cooled to room temperature at a rate of 1 °C min^{-1}. Shortly after that, the colorless microcrystal was obtained. The resulting sample was washed several times with fresh deionized water so as to remove the unreacted substance.

Powder X-ray diffraction (PXRD) experiments

Powder X-ray diffraction (PXRD) experiments were carried out to verify the structure and purity of $Zn_2(Atz)_2Ox$. Each PXRD pattern was recorded using a Rigaku SmartLab3 diffractometer (Cu Kα radiation, λ = 1.54178 Å) with a scan rate of

10°/min. The simulated powder pattern was obtained from Mercury 1.4.2 software.[5]

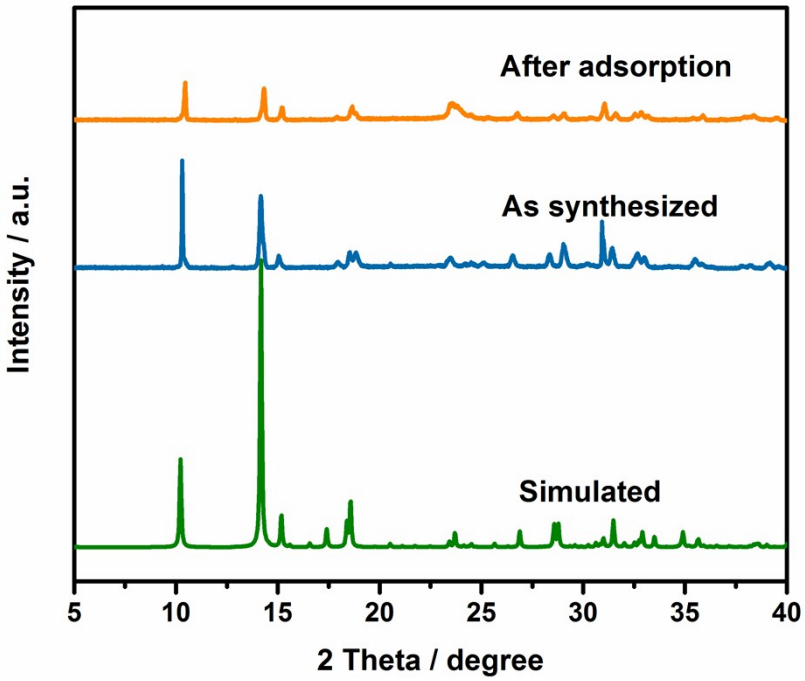

Fig. S1. PXRD patterns of as-synthesized $Zn_2(Atz)_2Ox$ (blue) and after-adsorption (orange) along with the simulated (green) pattern from the single-crystal X-ray structure.

Static adsorption measurements

As-synthesized samples of $Zn_2(Atz)_2Ox$ were dipped in fresh deionized water for 72 h, then degassed at 150 °C for 10 h under vacuum. By using a Micromeritics ASAP 2020 volumetric adsorption apparatus, the single component adsorption isotherms of C_2H_2, C_2H_4 and C_2H_6 on $Zn_2(Atz)_2Ox$ were recorded at 273, 298, 313, and 323 K. Bath temperatures of 298, 313, and 323 K were precisely controlled with a recirculating control system containing a mixture of ethylene glycol and water. The lower temperature (273 K) was controlled by a Dewar filled ice-water mixture.

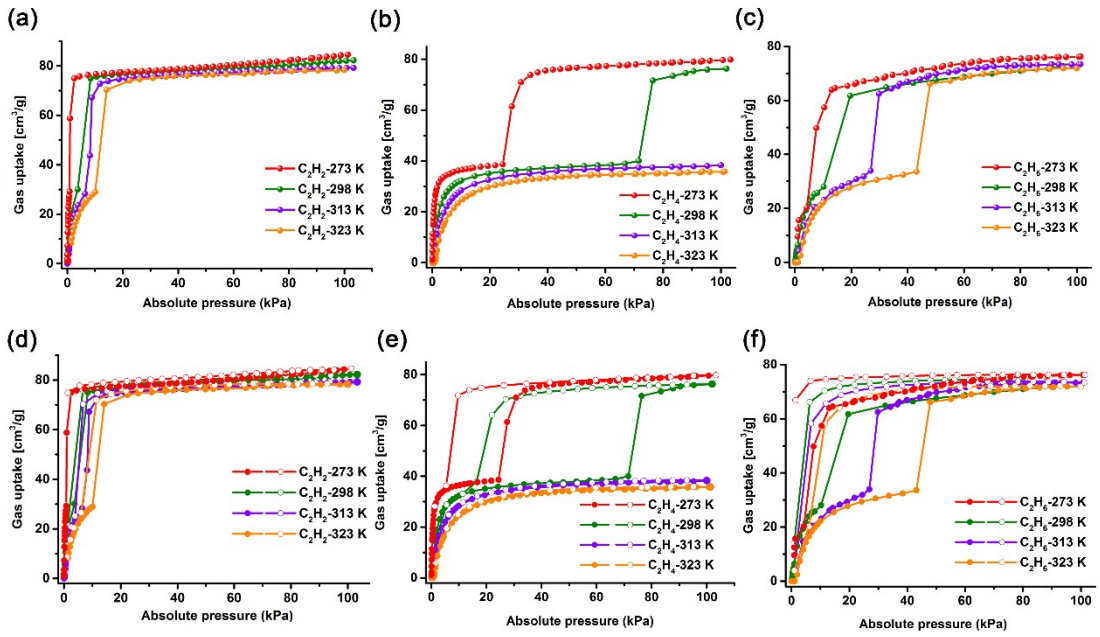

Fig. S2. Adsorption-desorption isotherms of (a, d) C_2H_2, (b, e) C_2H_4 and (c, f) C_2H_6 at 273 (red), 298 (green), 313 (purple), and 323 K (orange).

We noted that the $Zn_2(Atz)_2Ox$ exhibits large hysteresis loops for C_2 hydrocarbons, but not for CO_2.[6] According to the classification of hysteresis loops, the hysteresis loops of C_2 hydrocarbons in $Zn_2(Atz)_2Ox$ could be defined as type H1 loop, indicating that this process occurred in the pores corresponding to cylindrical shape channel model. In general, the adsorption hysteresis behavior can be attributed to the capillary condensation mechanism, which highly related with the characteristics of the adsorbate (kinetic size, saturated vapor pressure) and pore structure (size and shape). Interestingly, with the temperature increased to 313 and 323 K, the gate-opening and adsorption hysteresis behaviors of C_2H_4 disappeared in the range of measured pressures. This suggests that the final structure of $Zn_2(Atz)_2Ox$ after phase transition and the guest-framework interactions also play a vital role in triggering hysteresis phenomenon. Concretely, C_2 hydrocarbons possess slightly larger molecular size and stronger binding affinity compared with CO_2, resulting in higher desorption resistance. Meanwhile, C_2 hydrocarbons and CO_2 might show different packing states within the final pore structures due to different molecular geometries. As a linear molecule, CO_2 has a larger diffusion rate or higher desorption efficiency, which means that the structural basis for hysteresis will not be retained during desorption process.

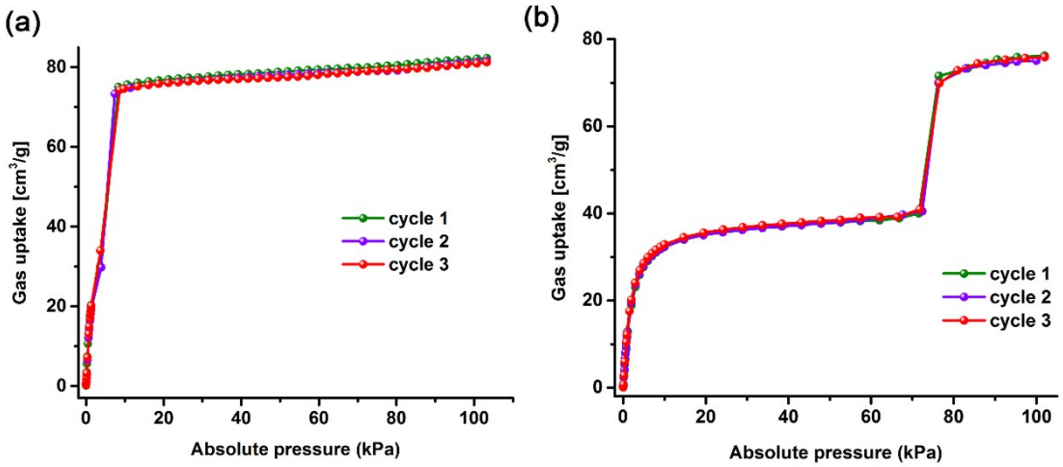

Fig. S3. Three cycles of (a) C_2H_2 and (b) C_2H_4 adsorption isotherms for $Zn_2(Atz)_2Ox$ at 298 K.

Calculation of isosteric heat of adsorption

In order to evaluate the bonding energy between C_2 hydrocarbons and $Zn_2(Atz)_2Ox$, the isosteric heat of adsorption was calculated according to the following equation:[7]

$$Q_{st} = -R\sum_{i=0}^{m} a_i N^i \quad (1)$$

$$\ln P = \ln N + \frac{1}{T}\sum_{i=0}^{m} a_i N^i + \sum_{j=0}^{n} b_j N^j \quad (2)$$

Here, P is the pressure (mmHg), T is the temperature (K), N is the adsorption amount in mg/g, a_i and b_j are Virial coefficients and m, n represent the number of coefficients used to adequately describe the adsorption curves. The values of a_0 through a_m were used to calculate the isosteric heat of adsorption using equation (1). Q_{st} is the coverage-dependent enthalpy of adsorption and R is the universal gas constant.

Calculation procedures of selectivity from IAST

Fitting details: The adsorption data was fitted with the single-site Langmuir-Freundlich equation at 298 K.

$$N = \mathrm{A} \times \frac{bP^c}{1 + bP^c} \quad (3)$$

Here, N is the adsorption amount in cm^3/g, P is the pressure of the bulk gas at equilibrium with the adsorbed phase (bar), A is the saturation loading of site A (cm^3/g), b is the affinity coefficients of site A (1/bar), c represents the deviations from an ideal homogeneous surface.

IAST selectivity calculation: Ideal adsorbed solution theory (IAST) enables prediction of adsorption equilibriums of the binary gas mixtures from the related single-component adsorption isotherms.[8] The selectivity for preferential adsorption of C_2H_2 over component C_2H_4 is defined as:

$$S_{\mathrm{ads}} = \frac{q_{\mathrm{C2H2}}/q_{\mathrm{C2H4}}}{y_{\mathrm{C2H2}}/y_{\mathrm{C2H4}}} \quad (4)$$

In the equation (4), q_{C2H2} and q_{C2H4} are the equilibrated adsorption molar loading of component C_2H_2 and C_2H_4; y_{C2H2}, and $y_{\mathrm{C2H4}} = 1\text{-}y_{\mathrm{C2H2}}$, represent the mole fractions of C_2H_2 and C_2H_4 in bulk gas phase.

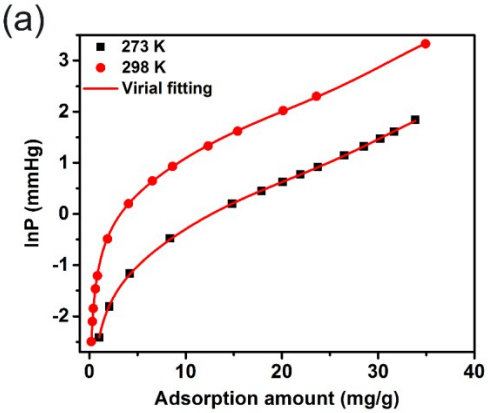

(b)

Qst (User)		
Adj. R-Square		0.99988
	Value	Standard Error
a0*	-4570.75308	51.87461
a1*	-13.8708	8.72953
a2*	4.08353	0.58226
a3*	-0.27926	0.04382
a4*	0.00755	0.00145
a5*	-7.49502E-5	1.70706E-5
b0*	14.42741	0.17502
b1*	-0.08015	0.02766
b2*	0.00304	8.78865E-4

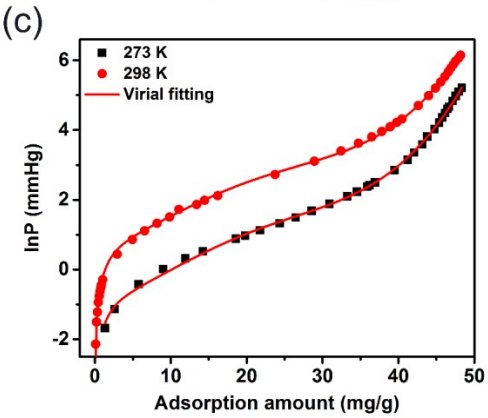

(d)

Qst (User)		
Adj. R-Square		0.99895
	Value	Standard Error
a0*	-4926.50371	189.02476
a1*	-53.30298	20.75851
a2*	6.31098	0.94908
a3*	-0.23787	0.04228
a4*	0.00405	9.51807E-4
a5*	-2.1943E-5	7.67936E-6
b0*	16.4878	0.63655
b1*	-0.03236	0.06251
b2*	-6.25554E-4	0.00118

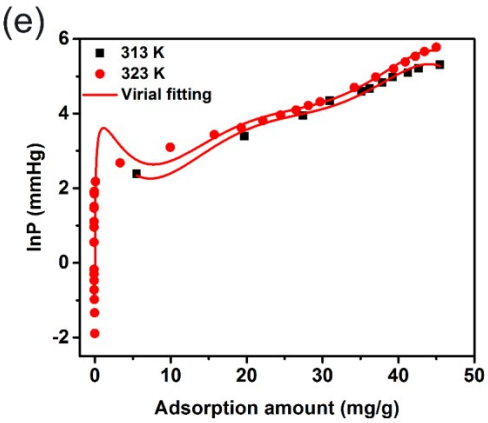

(f)

Qst (User)		
Adj. R-Square		0.86718
	Value	Standard Erro
a0*	-4659.2128	15890.54322
a1*	-28.71585	1355.72071
a2*	28.23632	34.8587
a3*	-1.51699	1.0017
a4*	0.03079	0.02338
a5*	-2.33687E-4	1.97278E-4
b0*	19.04051	49.14878
b1*	-1.02414	4.02537
b2*	0.02018	0.07527

Fig. S4. Virial fitting of (a) C_2H_2, (c) C_2H_4 and (e) C_2H_6 adsorption isotherms (points) at different temperatures. The related fitting parameters for (b) C_2H_2, (d) C_2H_4 and (f) C_2H_6 adsorption isotherms.

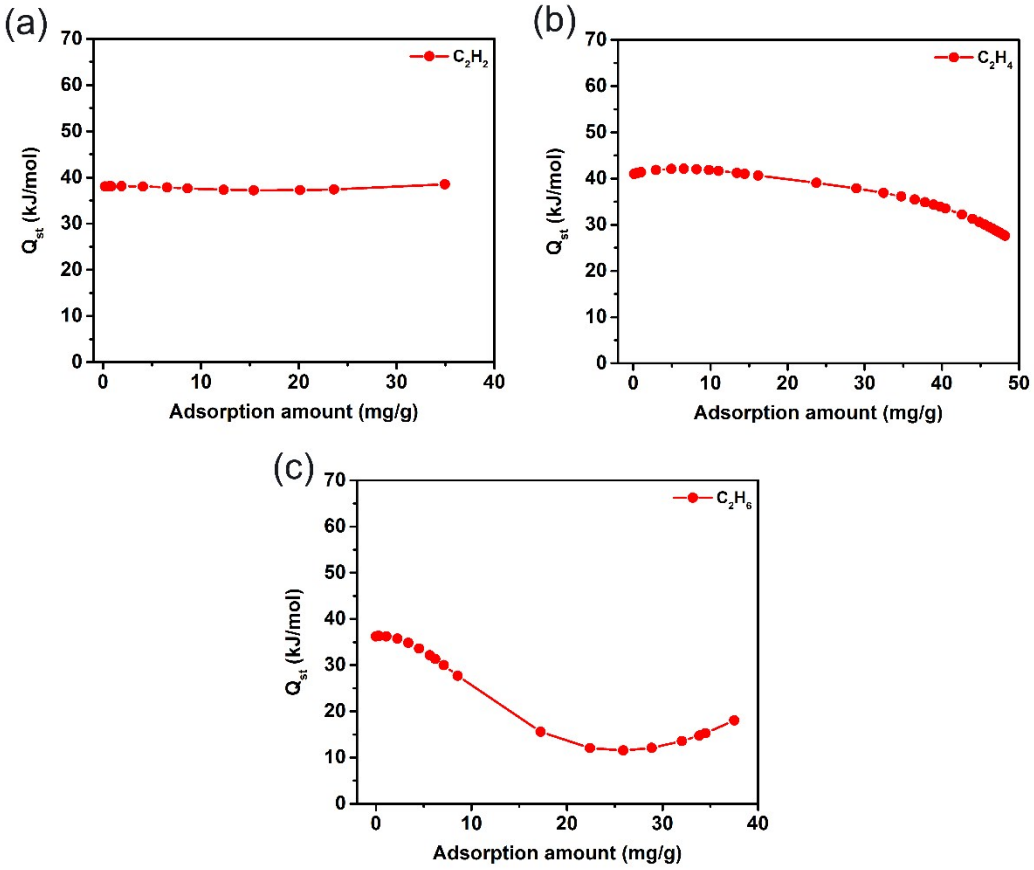

Fig. S5. Isosteric heats of adsorption of (a) C_2H_2, (b) C_2H_4 and (c) C_2H_6 at 298 K.

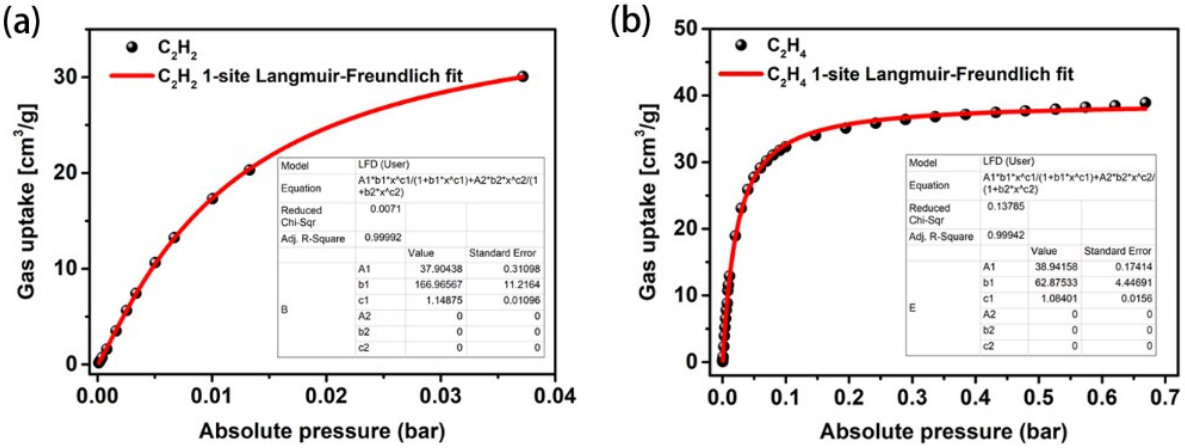

Fig. S6. Single-site Langmuir-Freundlich fitting (lines) of (a) C_2H_2 and (b) C_2H_4 adsorption isotherms (points) (298 K).

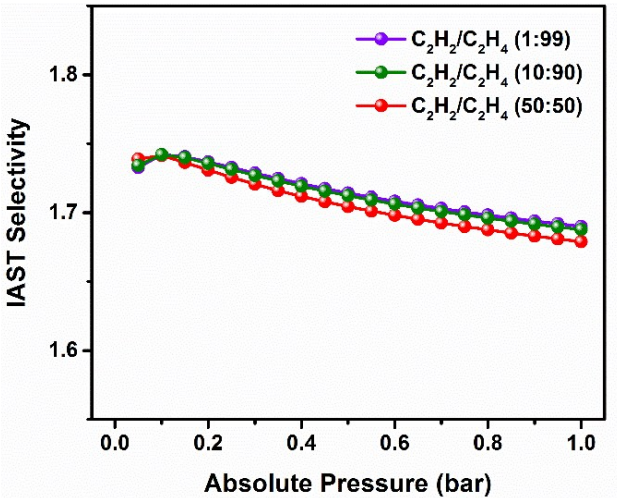

Fig. S7. The IAST selectivities of $Zn_2(Atz)_2Ox$ for C_2H_2 and C_2H_4 (1:99, purple; 10:90, green; 50:50, red) mixtures.

Column breakthrough measurements

Breakthrough experiments were executed by applying the separation column packed with 0.2 g activated $Zn_2(Atz)_2Ox$. The length of the column was 8 cm with an external diameter of 6 mm and an internal diameter of 4 mm. Before the breakthrough measurements, the sample was heated at 423 K for 8 h while the helium with a rate of 5 mL (STP) min^{-1} kept flowing. The feed gases, binary C_2H_2/C_2H_4 (50/50, v/v) and C_2H_4/C_2H_6 (50/50, v/v) mixtures, were supplied to this measurement with a flow rate of 4 mL (STP) min^{-1} under 298, 313, 323 K, and atmospheric pressure. The gas compositions at the outlet determined continuously by mass spectrometry (MS, Hiden,HPR-20). Other details of experimental devices were provided in Fig. S9.

Fig. S8. Photograph of the packing column.

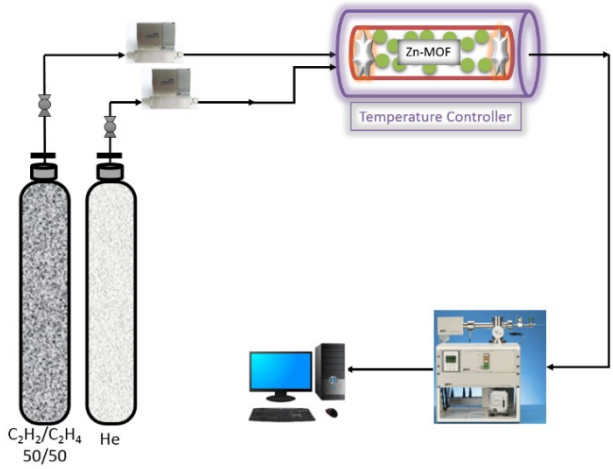

Fig. S9. Breakthrough experiment apparatus.

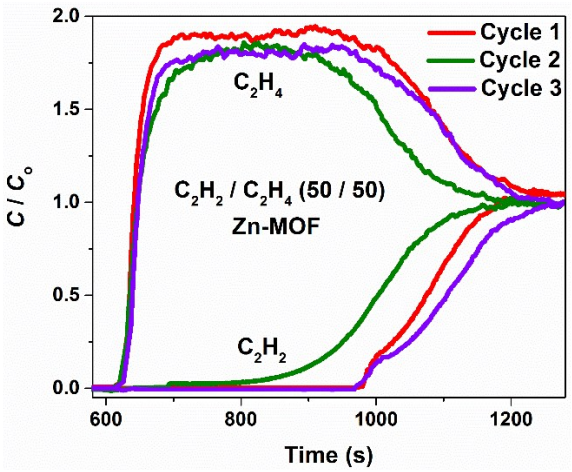

Fig. S10. Three cycles of dynamic column breakthrough curves of an equimolar C_2H_2/C_2H_4 mixture on $Zn_2(Atz)_2Ox$ at 298 K.

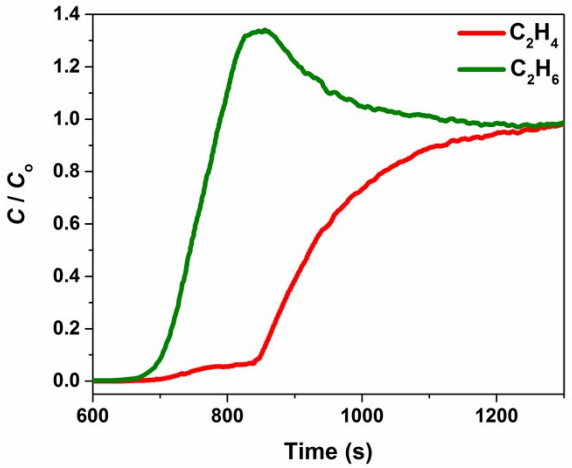

Fig. S11. Column breakthrough curves for an equimolar C_2H_4/C_2H_6 mixture carried out on $Zn_2(Atz)_2Ox$ at 298 K.

Clearly, the column breakthrough results for C_2H_2/C_2H_4 and C_2H_4/C_2H_6 mixtures carried out on $Zn_2(Atz)_2Ox$ are totally different. For the C_2H_2/C_2H_4 mixture, C_2H_2 molecule possesses several "advantages", including lower gate-opening pressure, smaller kinetic size and stronger binding affinity when compared to C_2H_4, which might synergistically promote the efficient separation of C_2H_2/C_2H_4. Particularly, although the IAST adsorption selectivity toward C_2H_2/C_2H_4 (50/50) was relatively low, the $Zn_2(Atz)_2Ox$ reserves its C_2H_2 uptake and partial separation ability during separation even when operated at 313 and 323 K. Furthermore, the breakthrough curves exhibit stepwise equilibrium and "roll-up" features, corresponding to the flexible responsive behaviors. Thus, the gate-opening effects might contribute more to breakthrough under 298 K in the case of C_2H_2/C_2H_4 mixture.

Besides, when we attempted to investigate the feasibility of the ternary $C_2H_2/C_2H_4/C_2H_6$ mixture separation in the $Zn_2(Atz)_2Ox$ under various conditions, the breakthrough experiments with multiple components (e.g., C_2H_4/C_2H_6/He: 10/90/0, 20/20/60) have been performed. The final results are very similar to that of C_2H_4/C_2H_6 (50/50) (partial C_2H_4 was captured by the column while C_2H_6 was detected in the outlet flow). This is consistent with the adsorption trend of C_2H_4/C_2H_6 before gate-opening and against the speculation based on critical pressures, which indicated that the guest-framework interactions or dynamic diffusion process might be the main influence factor of the breakthrough results for C_2H_4/C_2H_6 mixture under 298 K.

References

1 K. Jiang, L. Zhang, T. Xia, Y. Yang, B. Li, Y. Cui and G. Qian, *Sci China Mater.*, 2019, **62**, 1315.

2 C. R. Reid and K. M. Thomas, *J. Phys. Chem. B*, 2001, **105**, 10619.

3 C. E. Webster, R. S. Drago and M. C. Zerner, *J. Am. Chem. Soc.*, 1998, **120**, 5509.

4 A. Banerjee, S. Nandi, P. Nasa and R. Vaidhyanathan, *Chem. Commun.*, 2016, **52**, 1851.

5 Mercury 1.4.2, program for crystal structure visualisation and Exploration, Cambridge Crystallographic Data Centre, 12 Union Road, Cambridge CB2 1EZ, United Kingdom. Available from: http://www.ccdc.cam.ac.uk/.

6 A. Banerjee, S. Nandi, P. Nasa and R. Vaidhyanathan, *Chem. Commun*., 2016, **52**, 1851.

7 L. Li, R.-B. Lin, R. Krishna, H. Li, S. Xiang, H. Wu, J. Li, W. Zhou and B. Chen, *Science*, 2018, **362**, 443.

8 A. L. Myers and J. M. Prausnitz, *AIChE J*., 1965, **11**, 121.